Fully Connected Feedforward Neural Network for the Prediction of Amorphous Silicon Grating Couplers Efficiency

Daniel Almeida [1,2,3*], *Alessandro* Fantoni[1,2], *João* Costa[1,2], *Manuela* Vieira[1,2,3], and *José* Fonseca[2,3]

[1]ISEL-Instituto Superior de Engenharia de Lisboa, Instituto Politécnico de Lisboa, Portugal
[2]Center of Technology and Systems (UNINOVA-CTS) and Associated Lab of Intelligent Systems (LASI), 2829-516 Caparica, Portugal
[3]NOVA School of Science and Technology, NOVA University of Lisbon, 2829-516, Caparica, Portugal

Abstract. Photonic circuits are an enabling technology for the development of novel solutions in different fields such as healthcare, quantum computing, neural networks, communications, and manufacturing. Interconnections between devices and systems require low-loss light coupling strategies. Grating couplers are a promising solution to couple light between photonic circuits and optical fibres due to their off-plane coupling capabilities. Hydrogenated amorphous silicon (a-Si:H), which can be deposited by PECVD over a substrate of silica or glass, is a suitable low-cost solution for the production of such light coupling devices. In this work we developed, trained and tested a fully connected feedforward neural network for coupling efficiency prediction in a-Si:H grating couplers. The light coupling gratings were simulated by two-dimensional finite-difference time-domain (FDTD) analysis and field distributions were analysed with the Finite Element Method (FEM). Simulated gratings include non-apodized, linear and quadratic refractive index variation designs featuring full or partial etching, operating at 1550 nm. Not featuring any type of bottom reflector, the couplers exhibit coupling efficiencies up to about 40 % (~ -4 dB). The neural network multiclass grating coupler efficiency classifier was trained with over 3000 simulation results, reaching an accuracy over 85%, for coupling efficiencies between 0 and 30%+.

1 Introduction

Silicon photonic circuits are basic building blocks of several devices and systems finding applications in the fields of healthcare [1], communications [2], quantum computing [3], neural networks [4] and manufacturing. The design, simulation and optimization of photonic devices are expensive and time-consuming tasks, typically requiring high computational power. Of the three tasks, optimization can become the most challenging, due to the fact it usually requires the two previous steps to be redone. One of the simplest approaches consists in varying design parameters using an optimizer, which can be used to narrow down the possibilities and isolate the variables which are critical to achieve the best possible device performance, usually under human supervision.

The high computational power of modern graphics processing units (GPUs) and central processing units (CPUs) have the potential for being applied in highly demanding tasks, which are time and resource consuming, like photonic circuits' optimization. Artificial intelligence (AI), machine learning (ML) and particularly neural networks (NNs) are interesting tools for the research and development of photonic devices [5, 6], due to their power in the prediction of the outcomes of the typical workflow or in a reverse approach [7]. In other words, NNs can be used to either predict the performance of a given design or to start with an intended result and generate a possible candidate design. As examples, we have the works of Hammond and Camacho (2019) [8], which have successfully employed neural networks for modelling strip waveguides and chirped Bragg gratings and Miyatake et al. (2020) [9], that explored the utilization of NNs and the covariance matrix adaptation evolution strategy (CMA-ES), for the optimization of silicon-on-insulator (SOI) grating couplers (GCs). The particle swarm optimization method was successfully applied by Vitali et al. (2022) [10], for the optimization of dual-level silicon nitride grating couplers, based on two gratings (fully and partially etched) featuring opposite sign apodization.

Grating couplers, due to their off-plane coupling nature and high efficiency on near-infrared (NIR) wavelengths [11], constitute a flexible solution for photonic devices' interconnections. In this study, we trained a feedforward fully-connected neural network, for the prediction of the coupling efficiency of grating couplers composed of hydrogenated amorphous silicon (a-Si:H), deposited over a silicon substrate by low temperature plasma-enhanced chemical vapor deposition (PECVD), a low cost fabrication technique [12]. The grating couplers operate at the 1550 nm wavelength, both fully etched, and partially etched designs were simulated by 2D-FDTD. This work intends to demonstrate the applicability of artificial intelligence

* Corresponding author: dalmeida@deetc.isel.ipl.pt

(AI) and machine learning (ML), for the prediction of photonic circuits behaviour based on their design and setup parameters. By using neural networks to predict the behaviour of photonic components based on their design and configuration parameters it is possible to optimize and simplify the design procedure of new photonic solutions that can achieve better efficiency and performance.

2 Theory and Methodology

2.1 Amorphous Silicon Grating Couplers

The simulated grating couplers consist of a 220 nm thick hydrogenated amorphous silicon layer over a silica substrate, no bottom reflectors of any kind are included. Three different types of grating couplers are studied in this report: non-apodized gratings with fill-factors greater than 50 % (80, 85 and 90 %), apodized gratings featuring linear (negative slope) refractive index variation, and apodized gratings based on the quadratic variation of the refractive index [13]. All grating couplers and access waveguides have the same length, of 20.8 and 12 µm, respectively. Etching ratio was defined as 1 and 0.5 (100 % and 50 %), resulting in etch depths of 220 and 110 nm.

A total of 4950 bidimensional (2D) FDTD simulations were performed using the RSoft software package (Synopsys, Inc.), via University Donation Program [14]. Six input variables were swept, and the resulting coupling efficiency was measured, considering waveguide loss.

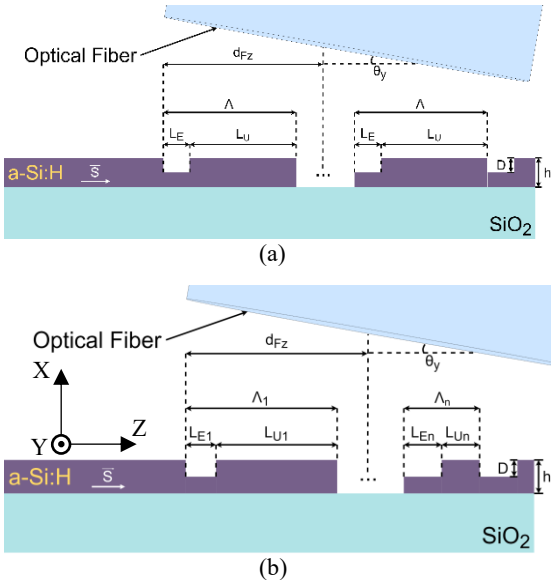

Fig. 1. Representation of the access waveguides, initial and final sections of the simulated grating couplers, showing geometrical design parameters and optical fibre positioning. Two types of grating coupler are represented: (a) Non apodized grating coupler with fill factor greater than 50 %; (b) Grating coupler with apodization, the fill factor and period (and consequently the refractive index) vary over the grating's length. The representation depicts coupler devices with a etch ratio of 50 % (110 nm etch depth).

Table 1. List of simulation variables and respective variation.

Parameter	Min.	Max.	Step
Coupling Angle (θ_y)	5°	15°	1°
Min. Fill Factor (F_{min})	50 %	70 %	5 %
Max. Fill Factor (F_{max})	80 %	90 %	5 %
Fiber Distance (d_{Fz})	3.2 µm	7.2 µm	1 µm
Variation Order (k)	0	2	1
Etch Ratio $(r = D/h)$	0.5	1	0.5

Grating coupler design and setup parameters that are fed to the NN are given as a span of integer and floating-point values, comprising start value, step and final value, as shown in Table 1. There are 7 input parameters in total. Grating coupler design parameters are diffraction angle (integer), maximum fill-factor (integer), minimum-fill factor (integer), effective refractive index variation order (integer), etch depth (float) and grating coupler height (float). The last two parameters are used in the calculation of the etch ratio (r). A setup parameter, the optical fibre offset along the grating coupler's length is also included as an input parameter, expressed as a floating-point value. Grating coupler and coupling configuration parameters are represented in Fig. 1, for designs with (b) and without (a) apodization. In Table 1, the simulation variables are presented along with the corresponding variations. The coupling angle (θ_y), or diffraction angle, corresponds to the angle formed between the plane of deposition and the coupling facet of the optical fibre, around the y axis, measured in units of degree (°). The fill factor is given as a ratio (between 0 and 1). Minimum fill factor (F_{min}) is only applicable to apodized gratings, maximum fill factor (F_{max}) is relevant for all grating designs. The fibre distance (d_{Fz}), corresponds to the distance measured between the grating's starting point (access waveguide's end) and the center of the optical fibre coupling facet, along the z axis, represented in units of micrometre (µm). Variation order (k) is the order of the grating coupler apodization along the z axis (0 means no apodization, 1 stands for linear refractive index variation and 2 for quadratic refractive index variation). The etch ratio (r), corresponds to the fraction of the etch depth (D) over the grating's height (h) and can take values between 0 and 1. The generic expression of the effective refractive index of the grating coupler along the z axis is given in (1).

$$n_{eff}(z) = \begin{cases} n_{eff}(0), & k = 0 \\ m \times z + n_{eff}(0), & k = 1 \\ a \times z^2 + b \times z + n_{eff}(0), & k = 2 \end{cases} \quad (1)$$

In expression (1), k is the variation order, $n_{eff}(0)$ corresponds to the grating's effective refractive index at its starting point, m is the slope in the linear variation of

the refractive index, in this work it always has negative sign, a and b are the coefficients of the quadratic function. Since the gratings covered in this work have decreasing refractive index along the z axis, a is always positive and b is always negative. The independent variable, z, is the distance along the z axis, in nanometer (nm), measured from the grating coupler's starting point.

2.1.1 Non-apodized Grating Couplers

The simplest grating coupler studied in this work is the non-apodized grating coupler with fill factor greater than 0.5 (or 50 %). The coupler device is constructed with the given values of fill factor (F_{max}) and coupling angle (θ_y), in this case, the variation order, k is defined as 0. The effective refractive index of the grating coupler is given by (2) [11]:

$$n_{eff} = F \times n_U + (1 - F) \times n_E \quad (2)$$

In expression (2), F, corresponds to the fill-factor, n_U is the effective refractive index of the unetched grating segment, which was calculated using FemSIM from RSoft (*Synopsys, Inc.*), as approximately 2.8209, the same value applies for the access waveguide. The parameter n_E corresponds to the effective refractive index of the etched grating segment, which was also obtained using FEM simulation, having a value of 2.1610, for a partially etched GC, with a etch depth of 110 nm (0.5 etch ratio), or 1.0000 for a fully etched GC, with an etch depth of 220 nm (1.0 etch ratio). The effective refractive index values were calculated considering the hydrogenated amorphous silicon GUTL model, as proposed by Fantoni *et al.* (2017) [15]. With the effective refractive index it is now possible to obtain the grating coupler's period from its effective refractive index, coupling angle and operating wavelength (in vacuum), expression (3) [11]:

$$\Lambda = \frac{\lambda_0}{n_{eff} - \sin\theta} \quad (3)$$

Where λ_0 is the wavelength in vacuum in units of nanometer (nm), θ (or θ_y in this case) is the coupling angle in degree (°) and Λ is the grating period in the same units as the wavelength (nm). The etched and unetched segment lengths are given by (4) and (5):

$$L_U = F \times \Lambda \quad (4)$$
$$L_E = (1 - F) \times \Lambda \quad (5)$$

Having all geometric design parameters of the non-apodized grating coupler, it can now be constructed, see Fig. 1(a).

2.1.2 Grating Couplers with Apodization

For grating couplers featuring apodization, expressions (2) and (3), must be modified to take into account the refractive index variation along the grating's length:

$$n_{eff}(z) = F(z) \times n_U + (1 - F(z)) \times n_E \quad (6)$$
$$\Lambda(z) = \frac{\lambda_0}{n_{eff}(z) - \sin\theta} \quad (7)$$

Now, the effective refractive index (n_{eff}), the fill-factor (F), and the period Λ, vary over the grating's length. In (6) and (7), z corresponds to the distance between an arbitrary point along the grating's length and the grating's starting point, measured in nanometer (nm). The other variables have the same values as described in the previous subchapter. Since the refractive index decreases over the coupler's length, and $n_U > n_E$, the maximum fill-factor (F_{max}) corresponds to the fill-factor of the first grating period ($F(0)$). Likewise, the minimum fill-factor (F_{min}) is the fill-factor of the last grating period ($F(L_{GC})$), where L_{GC} corresponds to the length of the grating coupler. To obtain the period ($\Lambda(z)$) and the fill-factor ($F(z)$) for the remaining grating periods, expression (1) is used, with $k = 1$, for 1st order (linear) refractive index variation, and $k = 2$, for 2nd order (quadratic) refractive index variation. Expression (8) is employed to obtain the linear variation slope ($k = 1$):

$$m = \frac{n_{eff}(L_{GC}) - n_{eff}(0)}{L_{GC}} \quad (8)$$

Where $n_{eff}(L_{GC})$, corresponds to the effective refractive index at the grating coupler's end, $n_{eff}(0)$ is the effective refractive index at the grating's starting point and L_{GC} is the length of the grating coupler in nanometer (nm). The slope of the GC effective refractive index function (m) is given in nm^{-1}. For the quadratic refractive index variation ($k = 2$), the following system of linear equations is defined (9):

$$\begin{cases} n_{eff}(L_{GC}) - n_{eff}(0) = a \times {L_{GC}}^2 + b \times L_{GC} \\ L_{GC} = -\dfrac{b}{2a} \end{cases} \quad (9)$$

Solving the system of linear equations to a and b, the following expressions result (10):

$$\begin{cases} a = \dfrac{n_{eff}(0) - n_{eff}(L_{GC})}{{L_{GC}}^2} \\ b = -2a \times L_{GC} \end{cases} \quad (10)$$

The coefficient a is given in units of nm^{-2} and the coefficient b is represented in units of nm^{-1}. With the coefficients of the quadratic function or the slope of the linear function it is possible to obtain $n_{eff}(z)$ from expression (1), which can be used to obtain all grating periods, by using expression (7) and setting z to the starting point of the nth grating period. The fill-factor can be obtained from (11), the unetched and etched GC segment lengths from (4) and (5), respectively:

$$F(z) = \frac{n_{eff}(z) - n_E}{n_U - n_E} \quad (11)$$

Having all geometric design parameters of the apodized grating couplers, these can now be constructed, refer to Fig. 1(b).

2.1.3 Optical Fiber and Photonic Waveguide

The simulated optical fibre employed in the grating couplers' efficiency performance tests is an SMF-28, which is commonly employed on the optical C-band

(1530-1565 nm), due to its ultra-low propagation loss, which is typically under 0.3 dB/km [16].

Typical core refractive index is approximately 1.4682 at 1550 nm, with a core-cladding index difference of 0.36% [16], which results in a cladding refractive index of about 1.4629 at 1550 nm. The SMF-28 has an average core diameter of 8.2 µm and a typical cladding diameter of 125 µm, the mean field diameter (MFD) is typically 10.4 µm at 1550 nm [16]. Due to this fact the grating length was set as twice the optical fibre MFD, or 20.8 µm (20800 nm) and the average fibre facet centre distance along the z axis, measured from the GC's starting point was set at one half MFD, or 5.2 µm (5200 nm).

The grating coupler efficiency corresponds to the overlap between the diffracted field at the fibre facet and the fundamental transverse electric (TE) mode of the optical fibre, expressed as a ratio (or percentage).

The effective refractive index of the fundamental transverse electric mode (TE_{00}) of the optical fibre, operating at a wavelength of 1550 nm is approximately 1.4669, the electric (E_y) and magnetic (H_x) field distributions are represented in Fig. 2(a) and (b), respectively.

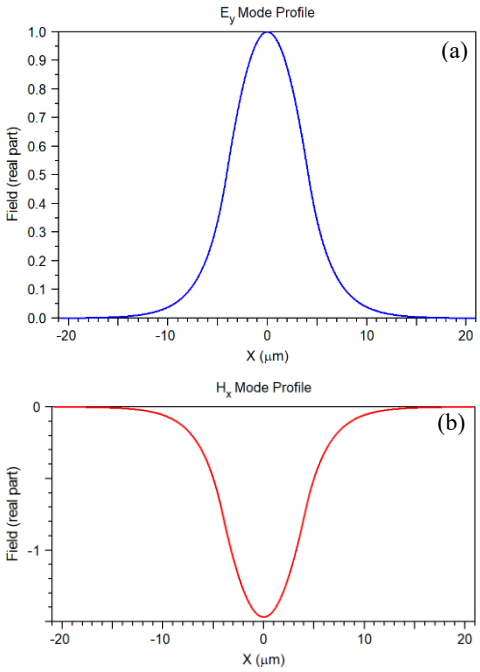

Fig. 2. Real component of the electric (a) and magnetic (b) fields of the simulated SMF-28 optical fibre, for the fundamental TE mode. In the horizontal axes, zero represents the centre of the optical fibre. Field amplitude, having its scale represented on the vertical axes is represented in arbitrary units.

The effective refractive index of the 220 nm a-Si:H photonic access waveguide was also calculated by the Finite Element Method (FEM), its value is approximately 2.8209, with an extinction coefficient of about 3.085×10^{-8}, for the quasi-TE fundamental mode (TE_{00}). The distributions of the electric (E_y) and magnetic (H_x) fields on the waveguide are represented in Fig. 3(a) and (b), respectively.

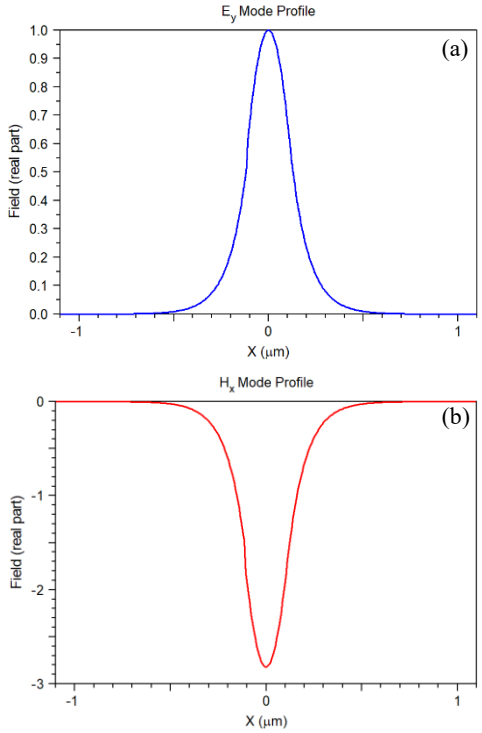

Fig. 3. Real component of the electric (a) and magnetic (b) field components of the photonic waveguide, for the fundamental quasi-TE mode. Amplitude, represented on the vertical axis is in arbitrary units. The horizontal scale represents the position, relative to the centre of the waveguide (zero), the a-Si:H layer is deposited from the right-side of the graphs over the silica layer, which starts at -0.11 µm, the air (cover) starts at +0.11 µm.

2.2 Neural Network

A feedforward fully connected neural network (NN) was trained with the input datasets from Table 1 and labeled with the efficiency results from the 2D-FDTD simulations. Input values were converted to floating point and normalized between 0 and 1, to prevent neuron saturation. The neural network implements a multiclass classifier, the labels were divided into 7 classes and fed to the NN as integer values between 0 and 6, having into account the GCs efficiency range:

- 0 to 5% (exc.),
- 5 to 10% (exc.),
- 10 to 15% (exc.),
- 15 to 20% (exc.),
- 20 to 25% (exc.),
- 25 to 30% (exc.),
- 30%+

The neural network features 2 layers with rectified linear unit (ReLU) activation functions, 2 with 2048 output neurons (Layer 1 and Layer 2) and a final layer with 7 output neurons (Layer 3), one per class, implementing a softmax activation function, which gives a statistical probability per each class, Fig. 4. The optimizer which yielded better implements the Adam (adaptive moment estimation) algorithm. For this classification problem the loss function of choice was defined as categorical crossentropy (i.e. the outputs are given as a fraction, whose sum equals 1). The learning rate was kept at the Keras' default value, of 0.001. Batch

size was set at 512, the power of two which resulted in the best training performance. The number of hidden layers was defined as 2, based on testing, each layer as 2048 neurons, a value corresponding to the power of two which yields the best neural network training and validation results, without excessively increasing complexity and training time.

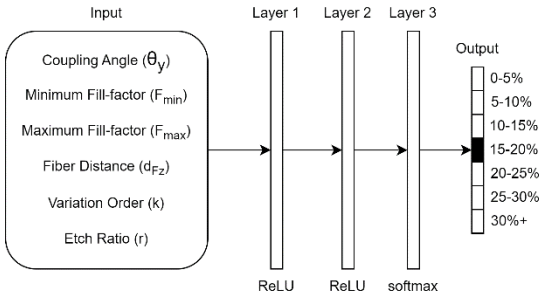

Fig. 4. Simplified diagram of the neural network used for grating coupler efficiency estimation based on design and setup parameters.

The simple feedforward neural network (NN) configuration was chosen to achieve the best computational cost vs. performance compromise. Due to its simplicity this NN is easier to replicate than more complex architectures. The NN was able to achieve a training accuracy in excess of 95 % and over 90 % validation accuracy. The NN is expected to run in modern central processing units (CPUs) and graphics processing units (GPUs), in machines with *TensorFlow* and *Keras* open-source machine learning platforms, running on Python environments. It can be trained for 100 epochs in under 8 seconds with a GeForce RTX 2080 Ti (*Nvidia Corp.*) GPU (with approximately 8.73 GiB of usable graphics memory and *TensorFlow* device compute capability 7.5) and in less than 22 seconds in an older GeForce GTX 1050 Ti (*Nvidia Corp.*) GPU (with around 2.7 GiB of usable graphics memory and *TensorFlow* device compute capability 6.1). To run *TensorFlow GPU 2.10.0* in *Nvidia Corp.* GPUs, the system must be configured with the Compute Unified Device Architecture (CUDA) API and CUDA Deep Neural Network (cuDNN). The NN architecture was tested with CUDA (*Nvidia Corp, Inc.*) 11.2.0, cuDNN (*Nvidia Corp, Inc.*) 8.1.0.77, Visual Studio Community 2019 (*Microsoft Corp.*) and Python 3.9.19.

3 Results and Discussion

3.1 Simulation Results

A total of 4950 bi-dimensional finite-difference time-domain (FDTD) simulations were performed, using the FullWAVE software tool from RSoft package (*Synopsis, Inc.*). A script written in Python language was necessary to dynamically design the grating couplers from the input parameters (Table 1). To avoid performance issues and bugs a *batch* script was written to perform variable sweep operations, instead of using the optimizer from the RSoft package (*Synopsis, Inc.*).

The simulation results are given as a fraction of input (launch) power, a positive floating-point value between 0 and 1, which can be expressed as a percentage. Two performance thresholds for apodized GC efficiency were defined for fully and partially etched gratings, of -3.9 dB (≈ 40.74 %) and -4.32 dB (≈ 36.98 %), respectively. Having into account such baselines, 7 fully etched and 5 partially etched designs were selected as achieving the top performance of the simulations' batch, Table 2.

Table 2. List of inputs which result in the best efficiencies for the apodized grating couplers, grey filled lines represent partially etched GCs, and white filed lines fully etched GCs. The meanings of the simulation/NN inputs are represented in Table 3.

Sim/NN Inputs						Efficiency
θ_y	F_{min}	F_{max}	d_{Fz}	k	r	
11°	55%	90%	5.2 µm	2	0.5	-4.311 dB
12°	50%	90%	5.2 µm	2	0.5	-4.309 dB
12°	55%	90%	5.2 µm	2	0.5	-4.312 dB
14°	55%	90%	6.2 µm	2	0.5	-4.297 dB
14°	60%	90%	6.2 µm	2	0.5	-4.316 dB
15°	55%	90%	6.2 µm	1	1	-3.827 dB
15°	60%	90%	6.2 µm	1	1	-3.751 dB
15°	60%	90%	7.2 µm	1	1	-3.887 dB
15°	65%	90%	6.2 µm	1	1	-3.759 dB
15°	65%	90%	7.2 µm	1	1	-3.691 dB
15°	70%	90%	6.2 µm	2	1	-3.879 dB
15°	70%	90%	7.2 µm	1	1	-3.777 dB

Table 3. List of simulation and neural network inputs (variables), represented in Table 2, associated with their respective meaning.

Sim./NN Input	Meaning
θ_y	Grating coupler diffraction angle
F_{min}	Minimum fill-factor
F_{max}	Maximum fill-factor
d_{Fz}	Fibre distance (from GC start)
k	GC refractive index variation: $k = 1$, linear $k = 2$, quadratic
r	Etch ratio ($r = D/h$)

Following a similar approach, two thresholds were set for non-apodized grating couplers. For fully etched grating couplers the limit was set at -4.8 dB (≈ 33.11 %), for partially etched designs the baseline was defined as -5.3 dB (≈ 29.51 %). Three designs of each etch ratio met such conditions, Table 4.

Table 4. List of inputs which result in the best coupling efficiencies for the design of non-apodized (constant refractive

index) grating couplers. Partially etched GCs are represented by the grey lines and fully etched GCs by the white lines. The meanings of the simulation/NN inputs are represented in Table 5.

Sim/NN Inputs				Efficiency
θ_y	F	d_{Fz}	r	
14°	80%	4.2 µm	0.5	-5.296 dB
14°	80%	5.2 µm	0.5	-5.200 dB
15°	80%	5.2 µm	0.5	-5.235 dB
14°	85%	5.2 µm	1	-4.765 dB
14°	85%	6.2 µm	1	-4.757 dB
15°	85%	6.2 µm	1	-4.724 dB

Table 5. List of simulation and neural network inputs (variables), represented in Table 4, associated with their respective meaning.

Sim./NN Input	Meaning
θ_y	Grating coupler diffraction angle
F	Fill-factor
d_{Fz}	Fibre distance (from GC start)
r	Etch ratio ($r = D/h$)

As can be observed, with this set of design parameters and optical fibre positioning, fully etched grating couplers exhibit better performance regarding efficiency, Table 3. The best apodized GC design is fully etched, with linear refractive index apodization, and achieves a coupling efficiency of approximately -3.691 dB (≈ 42.75 %). In contrast, the best apodized partially etched design, reaches an efficiency of around -4.297 dB (≈ 37.18 %), and features quadratic refractive index variation. The same is true for non-apodized grating couplers, Table 5, the best fully etched design achieves a coupling efficiency of about -4.724 dB (≈ 33.70 %). The best partially etched non-apodized GC exhibits an efficiency of approximately -5.2 dB (≈ 30.20 %).

Grating couplers with efficiencies over 30 % (≈ -5.229 dB), account for 872 designs, or about 17.62 % of all simulated devices. Having into account the percentage of simulation inputs and outputs reserved for NN training (72 % of all data), only around 244 designs remain for test and validation purposes. Due to this fact the highest classification which was attributed to the best performing devices was 30 %+. Of the 4950 simulations, 3564 are reserved for training, 396 for validation and 990 for test purposes. Data split ratio is 72 % (training), 8 % (validation) and 20 % (testing), this ratio is similar to that found in the textbook *Deep Learning with Python* (Chollet, 2021) [17]. The simulations are shuffled each time the neural network is trained, to assure better dispersion and to avoid training, validating or testing with a predefined data distribution, which could lead to poor training accuracy for the datasets with fewer occurrences, or incur in improper testing and/or validation.

3.2 Neural Network Training and Predictions

To establish the most appropriate number of training epochs, assuring an appropriate fit and avoiding overfitting or underfitting, training and validation loss and accuracy plots were drawn, Fig. 5(a) and (b). The traces were drawn until overfitting was evident, the neural network was trained for 540 epochs to obtain these performance metrics.

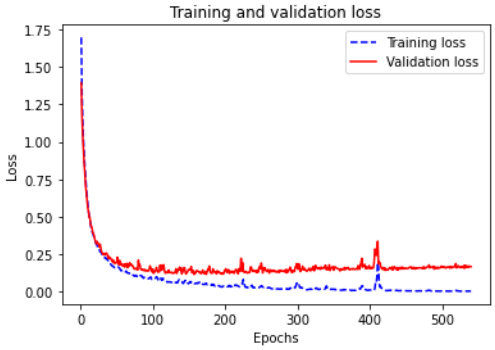

(a)

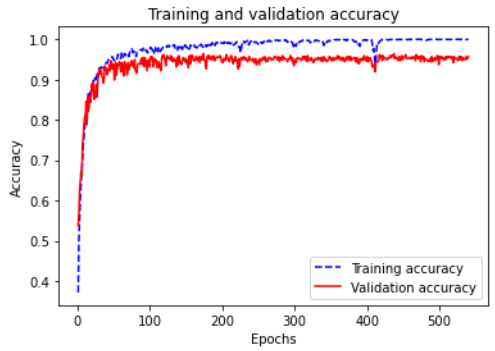

(b)

Fig. 5. Neural network training (dashed blue line) and validation (red line) loss (a) and accuracy (b) versus number of training epochs.

It can be noticed from the analysis of Fig. 5(a), that validation loss does not improve after about 100 training epochs, moreover, the line seems to slowly increase and diverge from the training loss line, this features mark the beginning of overfitting. Under about 50 training epochs both lines show a steep negative slope which clearly indicates underfitting. The same conclusions can be drawn from Fig. 5(b), where the validation accuracy does not (significantly) improve past the 100 epochs mark, and the training and validation lines start to diverge, showing overfitting. Under 50 training epochs the accuracy is clearly increasing, demonstrating underfitting.

In our perspective, the best fit occurs for 93 training epochs, or the average number of training epochs obtained with early stopping targeting validation loss with a patience of 10. For this number of training epochs, no non-adjacent target class classification errors were found, and test accuracy reaches an average value of 94.28 %, the average worst case classification accuracy (for the class with the lowest percentage of NN hits) is approximately 85.96 %. Numbers of training epochs below 93, demonstrated underfitting with the average measured test accuracy below 94 % and with an

average worst case classification accuracy under 85 %, non-adjacent class classification errors were found. Further training, for more than 134 epochs, results in overfitting, the training accuracy increases, but test accuracy is maintained slightly over the 94 % mark, on average. With an increase in the number of training epochs, a higher number of non-adjacent class classification errors were found.

Maximum learning accuracy is achieved between 444 and 540 epochs (on average), the first number was obtained by defining early stopping with training accuracy as target, and by setting the patience to a (very high) 100 epochs. The second number, 540 epochs, was the value which was found to give a higher percentage of 100 % training accuracy and the highest average for the same metric, which was found to be approximately 99.83 %. In fact, it is difficult to find the exact point where the NN reaches the highest training accuracy, since on each training cycle, the initial weights would be different, and the behaviour of the optimizer (Adam), may also differ slightly. Overfitting the model to the limit does not seem to bring any benefits.

A confusion matrix, displaying the "hits" and "misses" of the neural network, when trained for 93 epochs, is represented on Fig. 6.

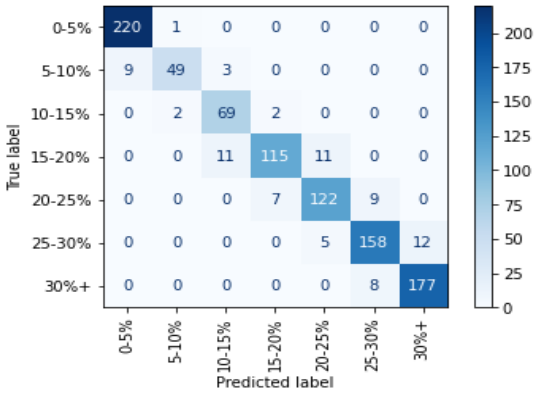

Fig. 6. Confusion matrix for an NN trained for 93 epochs, the test data has 990 occurrences. In this case test accuracy is around 95.35 % and the worst-case accuracy occurs for the 10-15% class, in which the NN have an accuracy of about 90.77 %.

The confusion matrix validates that a test accuracy of over 94 % and a worst-case accuracy of over 85 % are achievable, with a neural network properly dimensioned and trained to a near perfect fit.

4 Conclusion

A feedforward fully connected neural network, was successfully trained for the prediction of hydrogenated amorphous silicon (a-Si:H) grating couplers' efficiency, based on some of its setup and design parameters. The bidimensional (2D) finite-difference time-domain (FDTD) simulations, show that fully etched apodized grating couplers can achieve over -3.9 dB (≈ 40.74 %) coupling efficiency, and partially etched designs values above -4.4 dB (≈ 36.31 %). Non-apodized couplers can reach efficiencies over -4.8 dB (≈ 33.11 %), in fully etched designs and in excess of -5.3 dB (≈ 29.51 %), in the case of partially etched grating couplers. All devices are made by depositing a-Si:H over a silica substrate, which can be deposited by plasma-enhanced chemical vapor deposition (PECVD), at low temperatures, significantly reducing production costs. None of the devices feature any bottom reflector or mirror of any kind, nor any buried silicon layer.

The neural network, composed of two rectifier linear unit (ReLU) layers with 2048 output neurons and a final 7 neurons softmax output layer, when trained for 93 epochs, can achieve a classification accuracy of over 94 % and a worst-case accuracy above 85 %, while being compatible with older graphics processing units (GPUs). These results attest the relevance of neural networks for the prediction of grating couplers' efficiency, showing its potential for behaviour prediction of generic photonic circuits. The usage of machine learning for the predictability of grating coupler efficiencies, constitutes an important step for the design of more efficient photonic devices which can achieve better performance.

A downside of this study was the relatively low number of occurrences of grating couplers with coupling efficiencies over 30 %, which restricted the highest efficiency neural network class to 30 %+, and the number of classes to 7, instead of having the possibility of using 9 classes and two more classification intervals 30 % - 35%, 35 % - 40 % and 40 %+.

Acknowledgements

This research was supported by Portuguese national funds provided by FCT – Fundação para a Ciência e a Tecnologia, through grant SFRH/BD/07792/2021 (https://doi.org/10.54499/2021.07792.BD), funded by the Portuguese FCT program, Center of Technology and Systems (CTS) UIDB/00066/2020 / UIDP/00066/2020 and by FCT project ASER-META 2022.07694.PTDC.

References

1. Dhote, C., Singh, A., Kumar, S.: Silicon Photonics Sensors for Biophotonic Applications - A Review. IEEE Sens. J. 22, 18228–18239 (2022). https://doi.org/10.1109/JSEN.2022.3199663
2. Bernabé, S., Wilmart, Q., Hasharoni, K., Hassan, K., Thonnart, Y., Tissier, P., Désières, Y., Olivier, S., Tekin, T., Szelag, B.: Silicon photonics for terabit/s communication in data centers and exascale computers. Solid. State. Electron. 179, (2021). https://doi.org/10.1016/j.sse.2020.107928
3. Adcock, J.C., Bao, J., Chi, Y., Chen, X., Bacco, D., Gong, Q., Oxenløwe, L.K., Wang, J., Ding, Y.: Advances in Silicon Quantum Photonics. IEEE J. Sel. Top. Quantum Electron. 27, (2021). https://doi.org/10.1109/JSTQE.2020.3025737
4. Shastri, B.J., Huang, C., Tait, A., Ferreira de Lima, T., Prucnal, P.R.: Silicon photonic neural network applications and prospects. 52

(2022). https://doi.org/10.1117/12.2614865

5. Ma, W., Liu, Z., Kudyshev, Z.A., Boltasseva, A., Cai, W., Liu, Y.: Deep learning for the design of photonic structures. Nat. Photonics. 15, 77–90 (2021). https://doi.org/10.1038/s41566-020-0685-y
6. Jiang, J., Chen, M., Fan, J.A.: Deep neural networks for the evaluation and design of photonic devices. Nat. Rev. Mater. 6, 679–700 (2021). https://doi.org/10.1038/s41578-020-00260-1
7. Mao, S., Cheng, L., Zhao, C., Khan, F.N., Li, Q., Fu, H.Y.: Inverse design for silicon photonics: From iterative optimization algorithms to deep neural networks. Appl. Sci. 11, (2021). https://doi.org/10.3390/app11093822
8. Hammond, A.M., Camacho, R.M.: Designing integrated photonic devices using artificial neural networks. Opt. Express. 27, 29620–29638 (2019). https://doi.org/10.1364/oe.27.029620
9. Miyatake, Y., Sekine, N., Toprasertpong, K., Takagi, S., Takenaka, M.: Computational design of efficient grating couplers using artificial intelligence. Jpn. J. Appl. Phys. 59, (2020)
10. Vitali, V., Lacava, C., Domínguez Bucio, T., Gardes, F.Y., Petropoulos, P.: Highly efficient dual-level grating couplers for silicon nitride photonics. Sci. Rep. 12, 1–12 (2022). https://doi.org/10.1038/s41598-022-19352-9
11. Marchetti, R., Lacava, C., Khokhar, A., Chen, X., Cristiani, I., Richardson, D.J., Reed, G.T., Petropoulos, P., Minzioni, P.: High-efficiency grating-couplers: Demonstration of a new design strategy. Sci. Rep. 7, 1–8 (2017). https://doi.org/10.1038/s41598-017-16505-z
12. Fantoni, A., Costa, J., Lourenço, P., Vieira, M.: Computer simulation study about the dependence of amorphous silicon photonic waveguides efficiency on the material quality. EPJ Appl. Phys. 90, 1–10 (2020). https://doi.org/10.1051/epjap/2020190250
13. Almeida, D., Rossi, M., Lourenço, P.J.P.S., Fantoni, A., Costa, J., Vieira, M.: Amorphous silicon grating couplers based on random and quadratic variation of the refractive index. In: Proc. SPIE 12880, Physics and Simulation of Optoelectronic Devices XXXII, 128800J (11 March 2024). p. 38 (2024)
14. Synopsys Inc.: RSoft Photonic Device Tools, https://www.synopsys.com/photonic-solutions/rsoft-photonic-device-tools/rsoft-products.html
15. Fantoni, A., Lourenco, P., Vieira, M.: A model for the refractive index of amorphous silicon for FDTD simulation of photonics waveguides. Proc. Int. Conf. Numer. Simul. Optoelectron. Devices, NUSOD. 167–168 (2017). https://doi.org/10.1109/NUSOD.2017.8010044
16. Corning Inc.: Corning® SMF-28TM Optical Fiber, http://www.photonics.byu.edu/FiberOpticConnectors.parts/images/smf28.pdf
17. Chollet, F.: Deep Learning with Python. Manning Publications Co. (2021)